PCCP

Accepted Manuscript

ROYAL SOCIETY OF CHEMISTRY

www.rsc.org/pccp

Journal Name

ARTICLE

Even-odd product variation of the $C_n^+ + D_2$ (n = 4–9) reaction: Complexity of the linear carbon cation electronic states

Received 00th January 20xx,
Accepted 00th January 20xx

DOI: 10.1039/x0xx00000x

www.rsc.org/

K. Koyasu,[a,†] T. Ohtaki,[a] J. Bing,[b] K. Takahashi,[b*] and F. Misaizu[a]

We have studied reactions between linear C_n^+ (n = 4–9) and D_2, using ion mobility mass spectrometry techniques and quantum chemical calculations in order to understand complex reactivity of the linear cluster cations. Only linear C_nD^+ product was observed for the odd (n=5, 7, 9) linear clusters, while $C_nD_2^+$ was the main product for the even clusters. As for the reaction rate constants determined for these two channels, we have obtained the following two features: (1) the rate constant decreases with the size n, and (2) even-sized clusters have lower rate constants than neighboring odd-sized clusters. In the theoretical calculations using the CCSD(T) and B3LYP methods with the cc-pVTZ basis, we found that a low lying $^2\Sigma$ state in odd clusters may play an important role for these reactions. This is opposed to the previous interpretations that the $^2\Pi_{g/u}$ state is the dominant electronic state for linear C_n^+ (n = 4–9) clusters. We showed that a barrierless radical abstraction forming C_nD^+ occurs through direct head on approach for the $^2\Sigma$ state C_n^+. In contrast, a carbene-like insertion forming $C_nD_2^+$ occurs through a sideways approach for the $^2\Pi_{g/u}$ state C_n^+. We have concluded that the higher rate constants for the odd clusters come from the existence of symmetry broken $^2\Sigma$ states which are absent in even linear clusters.

Introduction

Due to flexible balance of s and p orbitals, carbon species are found in many different geometrical forms: linear chains[1], planar graphene[2], and three dimensional fullerene[3]. Recently, electronic states of linear chain polyynes have attracted scientists' interest because of the possible use in molecular electronic applications.[4] Furthermore, recent studies have shown the complexity of the electronic state at the "partial radical" graphene edges or in nanoribbons.[5] Due to interest in astrophysics[6] and combustion communities[7], many studies were performed on carbon clusters with focus on the effect of geometric structure towards the reactivity. Although there were a lot of studies on these clusters, understanding on the fairly complex electronic states is still lacking. Here we thus investigate the reactions of size and isomer selected carbon cation C_n^+ (n = 4–9) and D_2 with emphasis on electronic structure. There are numerous reviews on carbon clusters[8] because of the wide interest on these clusters[1–7], but we will just mention the studies that are pertinent to our present study in the following.

Using the Fourier transform (FT) ion cyclotron resonance (ICR) mass spectrometry, McElvany and coworkers[9] studied the reaction of size selected C_n^+ with D_2, O_2, HCN and simple hydrocarbons, while Parent[10] studied the C_nN^+ reaction with methane. These results showed an empirical rule that "for odd electron series of C_n^+ and C_nO^+, the odd n ions are more reactive than the even n ions"[9d]. For larger size clusters, Lifshitz and coworkers studied the reaction of C_n^+ with acrylonitrile.[11] Similarly, Bohme and coworkers[12] as well as Adams and Smith[13] utilized the selected ion flow tube method to study the reaction of C_n^+, C_nH^+, and C_nN^+ with CO, HCN, H_2, and simple hydrocarbons. Anderson and coworkers utilized the ICR method with an ion trap to perform single collision reactions of C_n^+ with D_2, O_2, or N_2O with controlled collision energies in the range of 0.1–7 eV.[14] The main conclusion obtained for the C_n^+ reaction in these studies is that the rate constant decreases with the cluster size, and in particular a large decrease was seen at n = 8 and 10.

Geometric structures of carbon clusters have also been investigated by photoelectron spectroscopy[15], infrared photodissociation[16], and electronic spectra of clusters captured in neon matrixes[17]. Bowers and coworkers utilized a drift tube ion mobility spectrometry[18] method and beautifully showed that the dominant geometry of C_n^+ changes from linear to cyclic, and cyclic to three dimensional fullerene around n = 10 and 30, respectively. This result provided

[a] Department of Chemistry, Graduate School of Science, Tohoku University, Aramaki-Aoba, Aoba-ku, Sendai 980-8578, Japan.
[b] Institute of Atomic and Molecular Sciences, Academia Sinica, P.O.Box 23-166, Taipei,10617 Taiwan R. O. C.
† Present address: Department of Chemistry, School of Science, The University of Tokyo, 7–3–1 Hongo, Bunkyo-ku, Tokyo 113–0033, Japan.

Electronic Supplementary Information (ESI) available: [Details concerning the experimental results, details on the quantum chemistry calculation of reactants and products, and details concerning the potential energy surface calculation, Figure of the ion spectrum of C_n^+, D adduct, D_2 adduct; comparison of reactivity of linear and cyclic C_9^+ ions; molecular orbitals for C_n^+ (n = 4–9) as well as the stable geometries of the C_n^+, C_nD^+ $C_nD_2^+$, and DC_nD^+, Table of the relative energies of C_n^+, C_nD^+ $C_nD_2^+$, and DC_nD, the frequencies for the D_2 adducts as well as comparison on the dissociation energy of the products are available in the supplementary material.]. See DOI: 10.1039/x0xx00000x

understanding on the decay of reactivity for the cluster sizes more than n = 10 mentioned above, i.e. cyclic isomers have smaller reactivity than linear chains. By mixing a small amount of reactant O_2 or NO molecules into the drift tube during the isomer separation, they proved that linear isomers have higher reactivity than that of cyclic isomers at the size less than n = 10.[18d] We also recently studied the isomer-specific dissociation reactions using this drift tube technique.[19]

On the theory side, elegant predictions were given by Mulliken[20], and by Pitzer and Clementi[21] on the spin state of neutral linear carbon clusters based on counting of σ and π orbitals. Raghavachari and coworkers confirmed that even clusters are singlet while odd clusters are triplet using quantum chemistry methods.[22] We note that a recent study showed that C_2 has a quadruple bonding character showing how closely the edge electrons interact.[23] While there have been numerous studies on the relative energies for the isomeric forms of neutral C_n[24], studies on cations have been much scarce.[25] Giuffreda et al.[26] performed density functional theory and coupled cluster calculation using double zeta basis, and Orlova and Goddard[27] studied the symmetry breaking in the linear odd chain cations. There have been several studies[28] on the calculation of excited electronic states to assign the electronic spectra taken by Maier and coworkers[17]. Utilizing photoionization spectrometry and theoretical calculations, Belau et al.[16] showed that the most stable electronic state for linear C_n^+ (n = 4–9) is $^2\Pi_{g/u}$ with the exception of C_5^+ which is $^2\Sigma_u$. As for reactivity studies, previous analysis on the reactivity of linear carbon clusters was based on thermodynamics where semiempirical method such as modified neglect of diatomic overlap were used to calculate the energies of reactant and products assuming $^2\Pi_{g/u}$ as the ground state.[9,10] In these calculations it was assumed that reactions of linear carbon cluster cations are similar to those involving carbenes, where an insertion reaction with D_2 will result in $C_nD_2^+$ which can fragment to C_nD^+ + D, as given in Figure 1(a). In this study, we also paid attention to another possibility: the radical abstraction reaction pathway that is given schematically in Figure 1(b).

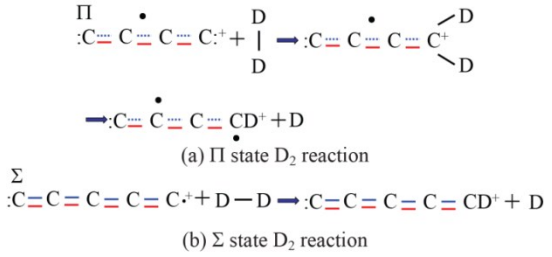

Figure 1. Schematics of the $C_n^+ + D_2$ reactions for the linear (a) Π and (b) Σ state C_n^+.

In the present study we have utilized an ion drift tube isomer separation method to perform detailed study on the size and isomer specific reaction rates for linear C_n^++D_2 (n = 4–9). Potential surface calculations were also utilized to obtain a deeper understanding on the cluster-size dependence in the reactivity.

Experimental and theoretical methods

Experimental methods. In this study, the chemical reaction of carbon cluster isomer ions was observed with an ion mobility mass spectrometer constructed in-house, which consists of a laser-vaporization cluster-ion source, an ion drift tube for isomer separation, and a reflectron time-of-flight (TOF) mass spectrometer. The details of this setup can be found elsewhere[19], and only a brief explanation will be given here. Carbon cluster ions were generated by laser-vaporization of a carbon disk with the second harmonic (532 nm) of a pulsed Nd:YAG laser and by cooling with pulsed He carrier gas (99.99995 %). The generated ions were injected with an energy of 200 eV into the ion drift tube, in which He was filled as a buffer gas and an electric field, 9.56 V cm^{-1}, was applied to guide the injected ions towards the exit of the cell. The separated isomers were then accelerated for mass-analysis in TOF mass spectrometer.

Information on cross sections and masses of the cluster ions were obtained in the present measurement of ion mobility mass spectrometry by following a previously reported procedure.[29] The timing of pulsed acceleration in the source of the TOF mass spectrometer was $t = t_0 + \Delta t$, in which t_0 and Δt represent the time for the injection into the cell and the time difference between the pulsed injection and acceleration of the ions, respectively. We hereafter call the time delay, Δt, as "arrival time". We thus obtained a series of TOF mass spectra sequentially as a function of Δt. The obtained mass spectra were plotted as a two-dimensional (2D) plot of Δt vs. TOF. Total TOF mass spectra were also obtained by summing up a series of TOF spectra at all Δt. We can also obtain a plot of arrival time distribution (ATD), in which the intensity of a certain TOF peak was obtained by summing up through a range of Δt, and plotted as a function of Δt. The peaks of the ATD plot correspond to representative arrival times of certain isomers of mass-selected ions.

The determined Δt was used to estimate a drift velocity, v_d, with which the ion mobility, K, was obtained as a ratio to the drift electric field, E ($K = v_d / E$). By using the theoretical formula given in the supplementary material (eq. S1), cross section, Ω, can be estimated from the reduced ion mobility, K_0, in which the number of density at the measurement condition of K was corrected to the value at the standard condition.

The reaction with D_2 was measured using a similar set up as those adopted by Bowers and coworkers[18] where D_2 gas was added in the drift tube as a mixture with He buffer gas in the concentration range of 0.1–1.0 %. This allowed us to measure the chemical reaction kinetics as well as to separate the isomer ions. Fluctuation of ion intensity during reaction measurement was compensated by normalizing with the intensity of the C_{11}^+ ion, which is regarded to be almost unreactive as noted later. Experimental errors of the C_n^+ intensity were estimated from plural independent measurements, except for C_4^+. We postulated that experimental errors in product-ion intensities are in the same order with those of the reactant C_n^+ ions. In our measurement, the experimental error for C_8^+ was larger than that of other sized clusters. Reaction rate constants were

determined by assuming that the reaction is a pseudo-first order reaction of D_2 concentration, and that the reaction time of the isomer ions are equivalent to the time in which the ions spend in the drift cell. This reaction time is determined from the arrival time of the ions. Experimental errors of the rate constants were estimated as 2σ of curve fittings, where σ represents standard deviation. The experimental error of n = 4 was estimated from the average of percentage of error for each size due to lack of data points for this size.

Under the present condition, the collision number with He in the cell was estimated from number density of He at 290 K and volume swept out by the C_n^+ ion. The volume was estimated from Ω, and the length of the cell, L = 0.10 m. For example, the collision number was 1.26×10^3 for C_9^+ and thus reactive collisions with D_2 was about 10 times in 1.0 % concentration.

Theoretical calculation methods. We performed geometry optimization for a full set of possible electronic states for the reactant: C_n^+, and products: C_nD^+, $C_nD_2^+$, and DC_nD^+. We note that for the present quantum chemistry calculation, we have assumed Born-Oppenheimer approximation and ignored the difference between H and D. For linear C_n^+, we considered the $^2\Pi_{g/u}$, $^2\Sigma_{g/u}$, $^4\Pi_{g/u}$, and $^4\Sigma_{g/u}$ states with $D_{\infty h}$ symmetry and the $^2\Sigma$ and $^4\Sigma$ states with $C_{\infty v}$ symmetry. For C_nD^+, we calculated the linear isomer with the D atom bound to the edge carbon for the $^1\Sigma$, $^3\Pi$, and $^3\Sigma$ states. This is because D adducts to other carbons have been reported to be endothermic.[9] Frequency calculations were also performed, in order to confirm that the calculated geometries for C_n^+ were stable minima. All the $D_{\infty h}$ ($C_{\infty v}$) calculations were performed with the D_{2h} (C_{2v}) symmetry calculation using the restricted open shell Hartree Fock (ROHF)[30] based unrestricted coupled cluster singles and doubles with perturbative triples (UCCSD(T))[31] method with Dunning's correlation consistent polarization valance triple zeta basis (cc-pVTZ)[32]. In addition, density functional calculation using the unrestricted Becke 3 parameter hybrid functional with Lee Yang Parr correlation functional (B3LYP)[33] using cc-pVTZ basis was also performed to confirm the accuracy of this B3LYP method. All the calculation was performed with the MOLPRO[34] program. In the following discussion only low lying electronic states will be mentioned and the remaining results will be summarized in the supplementary material.

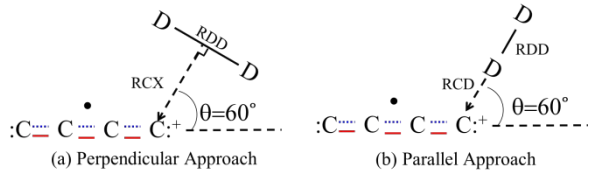

Figure 2. Schematics of the three effective coordinates for the $C_n^+ + D_2$ addition for (a) perpendicular and (b) parallel approach. In (a) collision coordinate RCX is the distance between the edge carbon and the center of the D_2, RDD is the D_2 bond length, and θ is the angle between the carbon chain and the RCX axis. Here the D_2 bond is perpendicular to the RCX axis, and the figure shows the situation at θ = 60˚. In (b) collision coordinate RCD is the distance between the edge carbon and the closer D atom of D_2, RDD is the D_2 bond length, and θ is the angle between the carbon chain and the RCD axis. Here the D_2 bond is parallel to the RCD axis, and the figure shows the situation at θ = 60˚.

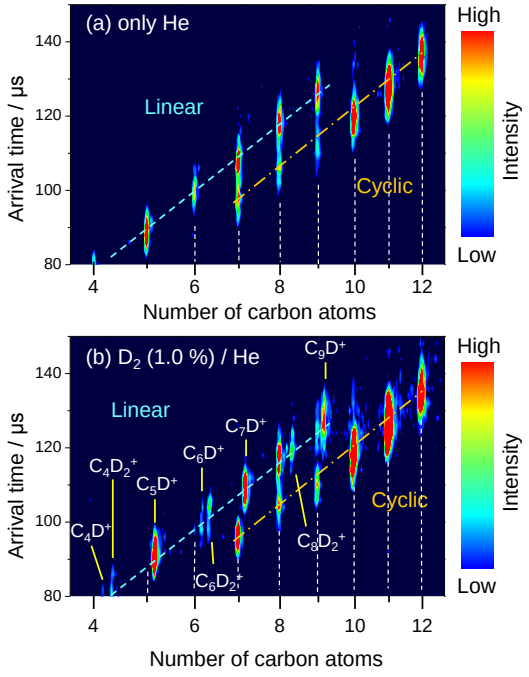

Figure 3. (color online) A typical arrival time -time of flight 2D plot using (a) only He and (b) 1.0 % D_2 in He as a buffer gas. The horizontal time of flight axis is converted into the number of carbon atoms. Linear and cyclic C_n^+ isomers are respectively indicated with blue dotted line and orange chain line. Positions of C_n^+ were shown with the white lines. Reaction products, $C_nD_x^+$ (x = 1 and 2) were also indicated.

Due to the strong attraction between the C_n^+ and D_2, we were not able to find any transition states for the reaction using B3LYP. To quantify the reaction process, we determined an effective reaction pathway using the B3LYP method in two directions for D_2 to approach C_n^+, namely, perpendicular and parallel. Using the three coordinates RDD (DD bond length), RCX (distance between the midpoint of D_2 and the edge carbon), and θ (angle between the linear carbon chain and RCX) given in Figure 2(a), we studied the energetics for the perpendicular approach by keeping all other degrees of freedom fixed. The applied constraints were as follows: 1. the orientation of the D_2 was fixed at perpendicular with respect to the RCX axis, 2. the C_n^+ was kept at the linear geometry with the bond lengths corresponding to those in the optimized geometry of the $\Pi_{g/u}$ state C_n^+, and 3. C_n^+ and D_2 were fixed to be in the same plane. In the parallel approach, we used RDD, RCD (distance between the edge carbon and the closer D atom of D_2) and θ (angle between the linear carbon chain and RCD) given in Figure 2(b). Similar to the perpendicular case, we fixed the plane of the two molecules, and the linear C_n^+ geometry was fixed to that of $^2\Sigma$ ($^2\Pi_{g/u}$) for odd (even) chains, while the D_2 axis was constrained to be parallel to RCD. See supplementary material for more details on the grid points for the three dimensional potential energy surface calculation.

After determining the critical regions for reaction from the three dimensional calculation using the B3LYP/cc-pVTZ method, we confirmed the energetics by calculating potential energy curves along this effective reaction path using the CCSD(T)/cc-pVTZ method. For the perpendicular approach at RCX = 1.3–2.4 Å we fixed θ at 80˚ and optimized RDD, while at RCX = 0.35–1.25 Å we fixed θ at 0˚ and optimized RDD. For the $^2\Sigma$ state odd linear cluster ions with parallel approach, we fixed θ at 0˚ and optimized RDD for RCD = 0.57–2.97 Å.

RESULTS and DISCUSSION

Isomer separated linear C_n^+ + D_2 reaction. Figure 3 shows a 2D contour plot of arrival time vs. number of carbon atoms in cluster cations, C_n^+, before (a) and after (b) reactions with 1.0 % of D_2 in He. In Fig. 3(a), we are able to distinguish different structural isomers by their arrival times, that is, two peaks at n = 7–9 can be assigned to the faster cyclic (short arrival time) isomers and the slower linear (longer arrival time) isomers, which is consistent with previous reports.[9,19] C_nD^+ and $C_nD_2^+$ were observed after reaction with D_2 at the right-hand side of each linear C_n^+ in Fig. 3(b).

With 1.0 % D_2 in the tube, the signal of the cyclic isomers were still observed as seen in Fig. 3(b), while the intensities of the linear isomers extensively decreased for n = 4–7 and 9. The fact that linear isomers react faster than cyclic ones is in accord with the previous notion that the linear species have reactive edges and form linear adducts, while the cyclic C_n^+ stay unreactive.[9,18] The signal intensities of the product ions of D adduct and D_2 adduct showed an even-odd alternation for n = 4–9. Odd linear C_n^+ generated only single D adduct ions. Linear isomers of C_4^+ and C_6^+ produced both single and double D adduct ions, while C_8^+ generated only double D adducts. Relative intensities of the product ions were confirmed from total TOF mass spectra, which was extracted by summing up all the TOF spectra obtained at every arrival time (see supplementary Fig. S1).

In order to discuss the reaction mechanism of C_n^+ with D_2, we investigated the D_2-concentration ([D_2]) dependence of the product intensity as shown in Fig. 4. The reactant shows a simple decrease for all n, while the single and double D adducts show monotonic rise except for n = 4. From D_2 concentration dependence, we also found that the reaction of cyclic isomers were much slower than the linear ones given in Fig. 4 (see supplementary material Fig. S2).

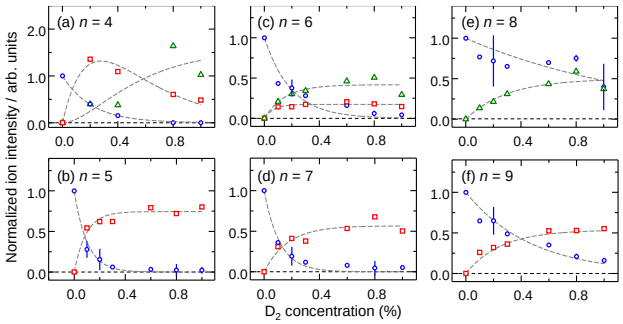

Figure 4. (color online) D_2 Concentration dependence of the product-ion intensities for even and odd linear C_n^+ ions. The reactants C_n^+, D adducts, and double D adducts are given in blue circles, red squares and green triangles, respectively. Fitting curves for decay of C_n^+, and growth of C_nD^+ and $C_nD_2^+$ were also given in gray dotted lines.

Possible reaction equations to generate C_nD^+ and $C_nD_2^+$ are expressed as:

(a) $C_n^+ + D_2 \rightarrow C_nD^+ + D$, addition on one side,

(b) $C_n^+ + D_2 \rightarrow C_nD_2^+$, addition on one side,

(c) $C_n^+ + D_2 \rightarrow C_nD^+ + D + D_2 \rightarrow DC_nD^+ + 2D$, addition on both sides.

The rate of the reaction type (a) and (b) should be proportional to D_2 concentration (Eq. S2), while for the reaction type (c) it is difficult to distinguish the order of reactions when the first step is much faster than the second step. Looking at our experimental results, the intensity of reaction products $C_6D_2^+$ is higher than that of C_6D^+ at all D_2 concentration region examined. This result indicates that C_6^+ reacts with D_2 under the type (b) rather than under the type (c). In the same way, $C_8D_2^+$ also seems to increase with the type (b). On the other hand, the reaction products from the odd C_n^+ clusters were only C_nD^+, indicating that the odd C_n^+ reacts with D_2 under the type (a), or stops at the first step in type (c).

Table 1 Comparison of the rate constants of D / D_2 adsorption on C_n^+.

Size, n	4	5	6	7	8	9
This study / 10^{-10} cm^3 s^{-1}	(2.7 ± 0.7)[d]	5.6 ± 0.9	2.3 ± 0.7	3.6 ± 0.7	0.28 ± 0.13	0.74 ± 0.16
McElvany et al.[9] / 10^{-10} cm^3 s^{-1}	3.24	4.5	1.35	1.89	0.063	0.410
Scott et al.[14] Cross section / Å	22.2[a]	33.3[a]	11.8[a]	4.20[b]	0.606[c]	2.73[d]

a: collision energy of 0.09 eV; b: collision energy of 0.10 eV; c: collision energy of 0.15 eV;

d: collision energy of 0.11 eV; d due to low intensity of C_4^+, the value was obtained from less number of data sets than the others.

Hence, we believe that we observed first order reactions under our present experimental conditions. Type (a) for odd and type (b) for even linear clusters except for C_4^+. However, this result is inconsistent with the previous report, in which the DC_nD^+ ions were produced by a successive reaction from C_n^+ in ICR cell directly after the generation with laser vaporization method.[9] This inconsistency may be due to the different reaction conditions. The ions generated in our reaction cell are cooled by collisions with 0.8 Torr of buffer gas, while the reactant ions used in the previous experiment were relatively hot following laser ablation. These experimental conditions indicate that different reaction mechanisms are active in the present experiment compared to the previous reports. Furthermore, the reaction time in the present drift tube, less than 0.1 ms, is shorter than the reaction time used in previous experiments[9]. In the previous ICR experiment, the reaction time can be extended from millisecond to several seconds.

For n = 4, the relative intensity change between D adduct and D_2 adduct implies that the reaction is more complicated; e.g. possibly including the secondary reaction of $C_4D^+ + D_2 \rightarrow DC_4D^+ + D$ mentioned in previous report.[9] Here, we should mention another possibility that $C_4D_2^+$ may be produced from the dissociation of $C_nD_2^+$, $n > 5$. In a previous collision energy controlled experiment, C_3-loss products, $C_{n-3}D^+$ were only observed at collision energy higher than 0.5 eV, while single D adduct C_nD^+ were only observed at low collision energies.[14a] Hence, we believe that the probability of C_3-loss products in our experiments is low based on the consideration that we have effectively cooled the reactant C_n^+ and the products by the He buffer gas in the drift tube with a temperature of 290 K, corresponding to collision energy of 0.1 eV at the maximum.

In Figure 5 and Table 1, we present a plot of the rate constants for n = 4–9 obtained from the parent ion decay in addition to the previous experimental results by McElvany and

Table 2. Relative energy of the low electronic states of even C_n^+ calculated by CCSD(T)/cc-pVTZ and B3LYP/cc-pVTZ. Possible products from primary collision reaction and secondary reaction are given in columns 4 to 6 and 7 to 9, respectively. For each n the results calculated by $C_{\infty v}$ symmetry are given below the dotted lines.

Size	Electronic state	Energy in eV	Primary Product	Electronic State	Energy in eV[a]	Secondary Product	Electronic State	Energy in eV[b]
C_4^+	$^2\Pi g$	0.00 (0.00)[c]	$C_4D_2^+$	$^2B_1$	–5.41 (–5.69)[c]			
			C_4D^++D	$^3\Pi$	–0.96 (–1.13)[c]	DC_4D^++D	$^2\Pi g$	–1.27 (–1.20)[c]
	$^4\Sigma g^-$	0.20 (0.25)[c]						
	$^4\Sigma u^-$	0.45 (0.49)[c]						
	$^4\Sigma^-$	*0.13 (0.25)[c]*	*C_4D^++D*	*$^3\Sigma^-$*	*–1.14 (–1.42)[c]*			
C_6^+	$^2\Pi u$	0.00 (0.00)[c]	$C_6D_2^+$	$^2B_1$	–4.87 (–5.12)[c]			
			C_6D^++D	$^3\Pi$	–0.55 (–0.59)[c]	DC_6D^++D	$^2\Pi u$	–1.07 (–0.94)[c]
	$^4\Sigma g^-$	0.58 (0.71)[c]						
	$^4\Sigma u^-$	0.61 (0.73)[c]						
	$^4\Sigma^-$	*0.57 (0.27)[c]*	*C_6D^++D*	*$^3\Sigma^-$*	*–0.89 (–1.11)[c]*			
C_8^+	$^2\Pi g$	0.00 (0.00)[c]	$C_8D_2^+$	$^2B_1$	–4.53 (–4.78)[c]			
			C_8D^++D	$^3\Pi$	–0.35 (–0.30[c]	DC_8D^++D	$^2\Pi g$	–0.99 (–0.79)[c]
	$^4\Sigma u^-$	0.72 (0.91)[c]						
	$^4\Sigma g^-$	0.73 (0.91)[c]						
	$^4\Sigma^-$	*0.54 (0.43)[c]*	*C_8D^++D*	*$^3\Sigma^-$*	*–0.76 (–0.94)[c]*			

a: relative energy for the reaction of $C_n^+ + D_2 \rightarrow C_nD^+ + D$ or $C_nD_2^+$;

b: relative energy for the reaction of $C_nD^+ + D_2 \rightarrow DC_nD^+ + D$;

c: relative energies obtained from the B3LYP/cc-VTZ level.

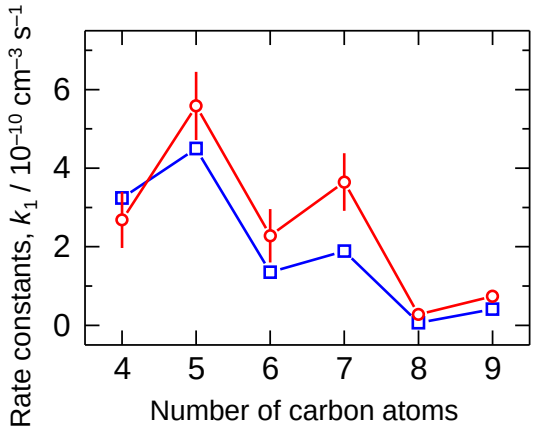

Figure 5. Cluster size dependence of the rate constant, k_1, for $C_n^+ + D_2$ is shown red circles with error bars. The rate constants from Ref. 9 (blue opened squares) are also shown for comparison.

coworkers[9] and Scott and coworkers[14a] (at collision energies of ~0.1 eV). We note that since Scott and coworkers performed single collision experiments, they obtained cross sections at give energies rather than the thermal rate constant obtained here. Thus direct comparison is not possible, but are presented in Table 1 to show the general trend. Formation rates of $C_8D_2^+$ and C_9D^+ were also estimated as discussed later. The fitting curve formulae of the decay and formation, shown as gray dotted lines in Fig. 4, are presented in the supplementary information. One can see from Fig. 5 the general trend that the reactivity for the linear carbon cation decreases as the increase of cluster size and showing a distinct minima at n = 8, which is consistent with the previous results[9b,14a,18]. The rate constants also show an even-odd alternation with even being smaller than odd. McElvany and coworkers[9b] also noticed this greater reactivity of odd species, and postulated that it is "due to structural differences or thermodynamic difference between reactant and product ions". Since the present experiment is specifically for linear clusters it cannot be due to structural differences.

Electronic structure calculation of C_n^+, C_nD^+, $C_nD_2^+$, and DC_nD^+. In order to understand the even–odd alternation in the main reaction products: C_nD^+ for odd versus $C_nD_2^+$ for even clusters, we obtained electronic structures of the linear carbon cluster cations by theoretical calculation, and discussed the reaction pathways based on the results. The relative energetics for the relevant reaction products of even and odd C_n^+ as well as their electronic states are summarized in the order of energy differences in Tables 2 and 3, respectively.

Our $D_{\infty h}$ symmetry calculations showed that the $^2\Pi_{g/u}$ states are the most stable for n = 4, 6–9 while $^2\Sigma_u$ is the lowest for C_5^+ in accord with the previous results[16]. At the optimized geometries for the low lying electronic states, we confirmed that the T1-diagnostics[35] were below the accepted value of 0.04 for the open shell species in the ROHF-UCCSD(T) calculations. Furthermore, the harmonic frequencies for C_n^+ showed no imaginary values signifying that the geometries are stable minima. Comparing even (Table 2) and odd (Table 3) linear C_n^+, we noticed that the energy difference between the $^2\Pi_{g/u}$ and $^2\Sigma_{g/u}$ states were fairly small for the odd C_n^+, which is consistent with previous calculations by Hochlaf et al. and Schnell et al.[28]

Next, we allowed bonds on both sides to have different lengths in the symmetry broken $C_{\infty v}$ calculation using ROHF-UCCSD(T)/cc-pVTZ. While the Π state C_n^+ structures were optimized to the respective symmetric geometries of $\Pi_{g/u}$, the Σ state C_n^+ structures converged to symmetry broken geometries. Such a possibility of symmetry broken solutions for the odd linear C_n^+ was reported previously.[26,27] The ROHF-CCSD(T)/cc-pVQZ optimized energies given in Table 3 are similar to those of cc-pVTZ, and thus the symmetry broken solutions are stable minima with this method. More details concerning the accuracy of the calculation methods, symmetry breaking, as well as vibrational frequencies are summarized in the supplementary material (Table S1-S3 and Figs. S3–S13). The important consequence of this symmetry broken solution is that the Σ state becomes the most stable electronic state only for the odd C_n^+ (italic numbers in Table 3). Computational proof on the validity of symmetry breaking requires multireference methods.[36] The research along this direction is being pursued, and it will be reported in the future.

Potential energy surfaces of $C_n^+ + D_2$. We calculated the potential energy surfaces of the $C_n^+ + D_2$ reaction to obtain a deeper understanding on the reaction mechanism. We examined the following two situations according to the schemes given in Fig. 2:

(1) D_2 addition with D–D bond perpendicular to the axis of approach to C_n^+ (Fig 2a)

(2) D_2 addition with D–D bond parallel to the axis of approach to C_n^+ (Fig 2b)

We plot the 2 dimensional contour potential energy cuts for the perpendicular approach as functions of RDD and θ at a fixed RCX for C_4^+ and C_5^+ in Figs. 6 (a) and (b), respectively. Here RDD, θ, and RCX represent functions of D–D internuclear distance, approaching angle, and C_n^+–D_2 collision coordinate, respectively. We only present results for C_4^+ and C_5^+, but all longer linear cluster ions also show similar behavior as given in supplementary material Figs. S14–S17. We also present the effective reaction path along RCX where RDD and θ are optimized while keeping the RCX fixed in supplementary material Figs. S18 and S19.

At large RCX values (RCX = 1.3 and 1.8 Å), the reaction proceeds by a sideways approach (θ = 70˚–90˚) with D_2 molecule keeping its gas phase equilibrium bond length of 0.74 Å. After passing RCX = 1.3 Å, θ quickly decreases to zero RDD gradually elongates in a barrierless manner. One can finally see the formation of the product, $C_nD_2^+$ at θ = 0˚ and RCX = 0.55 Å with an exothermicity of ~5 eV. Hence, the reaction path is more complex than a simple head on approach at θ = 0˚, and the complex reaction path is exactly the same as carbene insertion to a σ bond. For the simple H_2 insertion reaction to carbene, CH_2 ($^1A_1$) + H_2 → CH_4, Bauschechler et al.[37] mentioned that the head on (θ = 0˚) pathway is Woodward Hoffman orbital symmetry forbidden, resulting in a large

barrier. They also showed that a sideway approach θ = 90˚ leads to a barrierless pathway,[38] and Bach et al.[39] extensively analyzed similar systems.

Next, we examine the parallel approach for the $^2\Pi$ C_4^+ (a) and $^2\Sigma$ C_5^+ (b) as shown in Fig. 7. In the 2 dimensional potential energy cuts along the C_n^+–D_2 collision coordinate (RCD), a sideways (θ = 80˚) approach is favored for the $^2\Pi$ C_4^+. This is similar to the case in the perpendicular approach at RCH = 1.8 and 1.3 Å, while θ = 0˚ is favored at RCH < 1.3 Å. On the other hand, a barrierless encounter is favored along θ = 0˚ for the $^2\Sigma$ state C_5^+. For C_5^+, once RCD approaches 1.5 Å, RDD starts elongating without any barriers, and a smooth elongation of RDD causes formation of C_5D^+ + D for the $^2\Sigma$ C_5^+. Here we only discussed the results for C_4^+ but the general trend for longer even C_n^+ are similar to *n* = 4 and the same can be said between C_5^+ and longer odd C_n^+. (See supplementary material)

Since B3LYP may overestimate the intermolecular interactions[40], we also calculated the potential energy curves by the CCSD(T) method along the two reaction pathways: the perpendicular sideways path for $^2\Pi$ states (Fig. 8a) and the parallel head on path for odd $^2\Sigma$ states (Fig 8b). The general trend of CCSD(T) results matches those obtained by the B3LYP method, however one can clearly notice that a barrier is observed for *n* > 7 and this barrier increases with size in the perpendicular approach using the CCSD(T) level (Fig 8(a)).

Correlation between even-odd alternation of electronic states and experimental rate constants. We experimentally observed that even linear C_n^+ favor D_2 adduct ($C_nD_2^+$) while odd linear C_n^+ favor D adduct (C_nD^+) for the present first order reactions. For the experimental rate constant, we also observed an even-odd alternation along with decrease in the reactivity with increasing size *n*.

Previously, the ground electronic states of linear C_n^+ were assumed to be $^2\Pi_{g/u}$. The effective CCSD(T) potential energy curves for the $^2\Pi_{g/u}$ state reactions forming $C_nD_2^+$, Fig 8 (a), show that *n* = 4 and 5 are attractive while a small barrier is seen along this path by *n* = 6 and the barrier height steadily increases till *n* = 9. Therefore for this reaction path, one would expect a continuous decrease in the rate constant with increase in *n*. This is consistent with the previous notion that increase in *n* causes the radical electron to delocalize. This delocalization results in the decrease in the activity of the terminal carbon. However this contradicts with the experimentally observed even-odd alternation of rate

Table 3. Relative Energy of the low electronic states of odd C_n^+ calculated by CCSD(T)/cc-pVTZ and cc-pVQZ as well as with B3LYP/cc-pVTZ. Possible products for primary collision reaction are given in columns 4 to 6. For each *n* the results calculated by $C_{\infty v}$ symmetry are given below the dotted lines.

Size	Electronic state	Energy in eV	Primary Product	Electronic State	Energy in eV[a]
C_5^+	$^2\Sigma u^+$	0.00 [0.00][b] (0.00)[c]	$C_5D_2^+$	$^2A_1$	–4.21 (–4.37)[c]
	$^2\Sigma g^+$	0.09 [0.08][b] (0.08)[c]			
	$^2\Pi g$	0.25 [0.26][b] (–0.20)[c]	$C_5D_2^+$	$^2B_2$	–4.47 (–4.83)[c]
	$^2\Sigma^+$	*–0.24 [–0.25][b] (–0.53)[c]*	*C_5D^++D*	*$^1\Sigma$*	*–1.59 (–1.63)[c]*
C_7^+	$^2\Pi u$	0.00 [0.00][b] (0.00)[c]	$C_7D_2^+$	$^2B_2$	–4.39 (–4.80)[c]
	$^2\Sigma u^+$	0.08 [0.06][b] (0.59)[c]	$C_7D_2^+$	$^2A_1$	–4.06 (–4.18)[c]
	$^2\Sigma g^+$	0.09 [0.07][b] (0.60)[c]			
	$^2\Sigma^+$	*–0.22 [–0.24][b] (–0.02)[c]*	*C_7D^++D*	*$^1\Sigma$*	*–1.52 (–1.57)[c]*
C_9^+	$^2\Pi g$	0.00 [0.00] [b] (0.00)[c]	$C_9D_2^+$	$^2B_2$	–4.30 (–4.56)[c]
	$^2\Sigma u^+$	0.26 [0.24][b] (0.81)[c]	$C_9D_2^+$	$^2A_1$	–3.97 (–3.85)[c]
	$^2\Sigma g^+$	0.26 [0.24][b] (0.81)[c]			
	$^2\Sigma^+$	*–0.07 [–0.09][b] (0.18)[c]*	*C_9D^++D*	*$^1\Sigma$*	*–1.47 (–1.33)[c]*

[a]: relative energy for the reaction of C_n^++D_2→C_nD^++D or C_nD_2

[b]: relative energies obtained from the cc-VQZ basis set.

[c]: relative energies obtained from the B3LYP/cc-VTZ level.

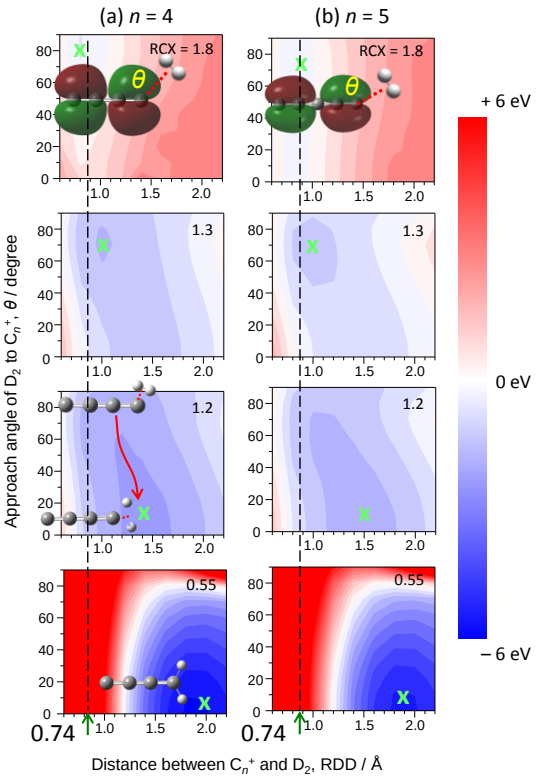

Figure 6. (Colour online) Potential energy surface for perpendicular approach for the D_2 addition to (a) C_4^+ and (b) C_5^+ at RCX = 1.8, 1.3, 1.2, and 0.55 Å calculated by B3LYP/cc-pVTZ. The carbon bond lengths are fixed at the equilibrium value of linear C_n^+ in the $\Pi_{g/u}$ state. Schematic structure for the approach is presented in the C_4^+ results. Each contour line corresponds to 0.5 eV and the region given in red, white, and blue corresponds to energies greater than, equal to, and lower than the total energy of $^2\Pi_{g/u}$ C_n^+ and D_2 at infinite separation, respectively. Refer to the web version for the colored version of the figure.

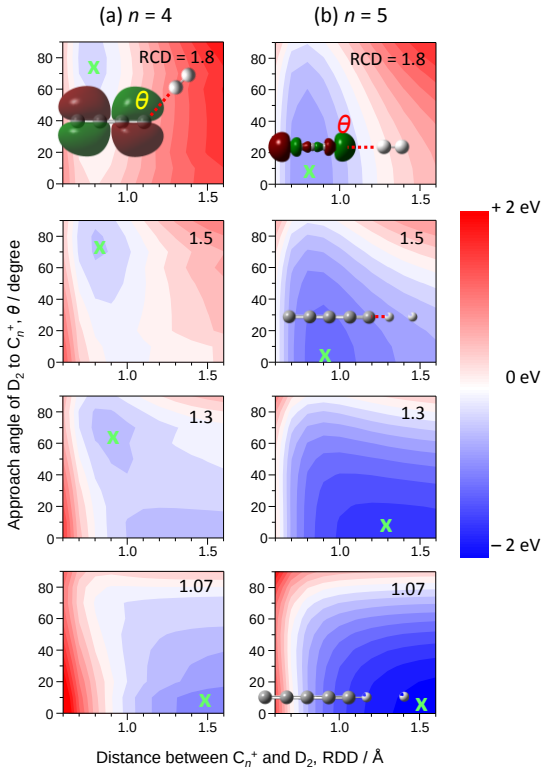

Figure 7. (Colour online) Potential energy surface for parallel approach for the D_2 addition to (a) $^2\Pi_g$ C_4^+ and (b) $^2\Sigma$ C_5^+ at RCD = 1.8, 1.5, 1.3, and 1.07 Å calculated by B3LYP/cc-pVTZ. The carbon bond lengths are fixed at the equilibrium value of linear $^2\Pi_g$ C_4^+ and $^2\Sigma$ C_5^+. Schematic structure for the approach is presented in the C_5^+ results. Each contour line corresponds to 0.2 eV variation and red, white, and blue region corresponds to energies higher than, equal to, and lower than the total energy of C_n^+ and D_2 at infinite separation, respectively. Refer to the web version for the colored version of the figure.

constants given in Fig 5.

Indeed n = 9 is more reactive than n = 8, and this can also be seen by comparing the experimental product formation rate of $C_8D_2^+$ (0.96×10^{-11} cm^3 s^{-1}) versus C_9D^+ (1.46×10^{-11} cm^3 s^{-1}). Thereby, we believe that C_9D^+ formed from C_9^+ is not a dissociation product of $C_9D_2^+$ generated from $^2\Pi_g$ C_9^+. On the other hand, the potential energy curves for the odd Σ state radical abstraction given in Fig 8 (b) have almost no barriers even for the longer n = 7 and 9 ions. Thereby we conclude that the radical abstraction by the $^2\Sigma$ state (see Fig 1(b)) forming C_nD^+ is responsible for the observed larger reactivity of the odd linear C_n^+ compared to even species. The physical reason is that due to the symmetry breaking, the odd C_n^+ has single occupied radical terminal orbitals which protrude out (see ESI Fig S10) to attract the D_2. However, as n increases, this protrusion decreases due to the delocalization in the carbon chain, thus the attraction decreases as seen in Fig 8b. Theoretical rate constants based on statistical unimolecular reaction model for the C_n + D_2^+ reaction using multireference potential energy surfaces should provide a direct comparison with the experimental values, and will be examined in future works. Lastly, although we did not consider the difference due to the mass of D_2 and H_2, we believe that for the present barrierless reaction the kinetic isotope effects will be small, and this will also be verified in our future work.

CONCLUSION

Using the ion mobility spectrometry techniques, we separated the linear and cyclic isomers to specifically study the C_n^+ (linear) + D_2 reaction (n = 4–9) in detail. While for the even linear cations we were able to detect both C_nD^+ and $C_nD_2^+$ products, we could only detect the C_nD^+ product for the odd linear cluster ions. Furthermore, even-odd alternation in the reaction rate constants was observed where the latter was slightly more reactive than the former.

From the systematic analysis for C_n^+ using the CCSD(T) and B3LYP functional with cc-pVTZ basis set, we showed that the symmetry broken $^2\Sigma$ is the lowest electronic state for odd C_n^+ while $^2\Pi_{g/u}$ states are slightly higher in energy. Theoretical potential energy surfaces were used to clarify that a carbene like insertion forming $C_nD_2^+$ occurs through the perpendicular sideways approach (θ = 80˚) for the $\Pi_{g/u}$ state C_n^+. As for the Σ state C_n^+ a radical abstraction forming C_nD^+ occurs through parallel direct head on approach (θ = 0˚). As a conclusion the even linear ions with $^2\Pi_{g/u}$ as the ground electronic state is likely to react to form $C_nD_2^+$, while the odd linear ions with symmetry broken $^2\Sigma$ as the ground state react to form C_nD^+, which is consistent with the experimental result that only C_nD^+ product is observed for odd, with a larger rate constants. Similar sensitivity of the electronic state has been reported for the reaction of C_2H_3 with H_2. Mebel et al.[41] reported that the unpaired σ electron can abstract a hydrogen atom forming

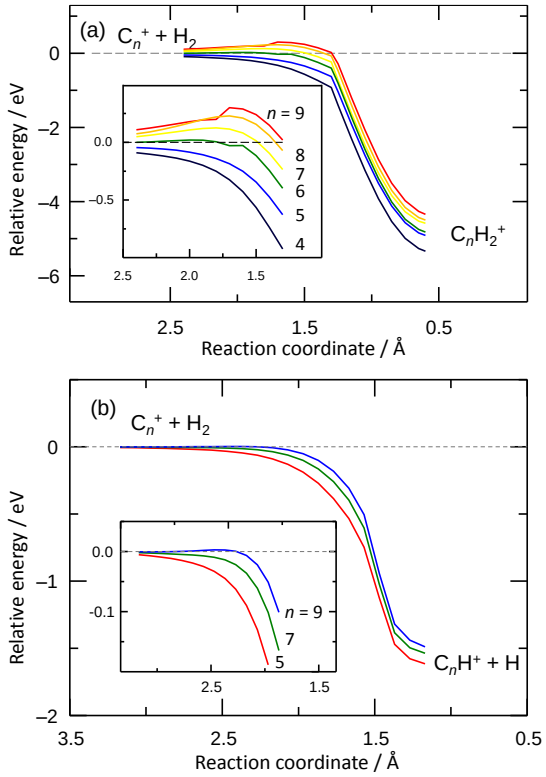

Figure 8. Effective potential energy curve for D_2 addition for (a) perpendicular approach to $^2\Pi$ C_n^+ (n = 4–9) and (b) parallel approach for odd $^2\Sigma$ C_n^+ (n = 5, 7, 9) calculated by CCSD(T)/cc-pVTZ. In (a) other coordinates are fixed at the equilibrium value of the linear C_n^+ in the Π state, while in (b) other coordinates are fixed at the equilibrium value of the linear C_n^+ in the Σ state. Expanded views of the curves around potential barrier are presented as insets with numbers of carbon atoms.

C_2H_4, but will not insert into the hydrogen molecule for direct production of the more exothermic product: C_2H_5.

Lastly, while previous analysis on linear C_n^+ reactivity has been based on geometric structure arguments, we presently conclude that the electronic structure is also an important factor to understand reactivity of C_n^+ from the detailed isomer separated reaction experiments and quantum chemistry calculations on the reaction path. We think that this complex electronic state of the linear C_n^+ may be imprinted in the reaction with other simple molecules such as O_2, HCN and research along this direction is being pursued. In addition, for the short linear even C_n^+, especially n = 4, the $^4\Sigma$ state lies very close in energy to the $^2\Pi$ states and is probably responsible for the observed complex behavior for this chain length and more detailed studies are being performed to understand the effect of spin states on the reaction.

Acknowledgements

This work was supported by Yamada Science Foundation, Sumitomo Foundation, and in part by a Grant-in-Aid for Scientific Research from the Japan Society for the Promotion of Science (JSPS). KT thanks Academia Sinica, National Center for High Performance Computing of Taiwan and Ministry of Science and Technology of Taiwan (Grant: NSC 102-2113-M-001 -012 -MY3) for support.

References

1 W. A. Chalifouz and R. R. Tykwinski, *Nature Chem.* 2010, **2**, 967–971.
2 K. S. Novoselov, A. K. Geim, S. V. Morozov, D. Jiang, Y. Zhang, S. V. Dubonos, I. V. Grigorieva and A. A. Firsov, *Science* 2004, **306**, 666-669.
3 H. W. Kroto, J. R. Heath, S. C. O'Brien, R. F. Curl and R. E. Smalley, *Nature* 1985, **318**, 162-163.
4 P. Moreno-Garcia, M. Fulcur, D. Z. Manriqui, T. Pope, W. Hong, V. Kaliginedi, C. Huang, A. S. Batsanov, M. R. Bryce, C. Lambert and T. Wandlowski, *J. Am. Chem. Soc.* 2013, **135**, 12228-12240.
5 (a) K. Suenaga and M. Koshino, *Nature* 2010, 468, 1088-1090. (b) D. E. Jiang, B. G. Sumpter, and S. Dai, *J. Chem. Phys.* 2007, **126**, 134701. (c) Z. Chen, D. E. Jian, X. Lu, H. F. Bettinger, S. Dai, P. v. R. Scheleyer and K. N. Houk, *Org. Lett.* 2007, **9**, 5449-54552. (d) Y. W. Soh, M. L. Cohen, and S. G. Louie, *Nature* 2006, **444**, 347-349. (e) F. Plasser, H. Pasalic, M. H. Gerzabek, F. Libisch, R. Reiter, J. Burgorfer, T. Muller, R. Shepard, and H. Lischka, *Angew. Chem. Int. Ed.* 2013, **52**, 2581-2584. (f) W. Mizukami, Y. Kurashige and T. Yanai, *J. Chem. Theo. Comput.* 2013, **9**, 401-407.
6 (a) P. F. Bernath, K. H. Hinkl, and J. J. Keady, J. J. *Science* 1989, **244**, 562-564. (b) M. C. McCarthy, M. J. Travers, A. Kovacs, C. A. Gottilieb, and P. Thaddeus, *Astrophys. J. Suppl. Series* 1997, **113**, 105-120. (c) Y. J. Wu, H. F. Chen, C. Camacho, H. A. Witek, S. C. Hus, M. Y. Lin, S. L. Chou, J. F. Oglive, and B. M. Cheng, *Astrophys. J.* 2009, **708**, 8-11. (d) O. Kostoko, J. Zhou, B. J. Sun, J. S. Lie, A. H. H. Chang, R. I. Kaiser, and M. Ahmed, *Astrophys. J.* 2010, ***717***, 674-682. (e) R. I. Kaiser, B. J. Sun, H. M. Lin, A. H. H. Chang, A. M. Mebel, O. Kostko, and M. Ahmed, *Astrophys. J.* 2010, **717**, 1884-1889. (f) N. Sakai, T. Sakai, T. Hirota, and S. Yamamoto, *Astrophys. J.* 2010, **722**, 1633-1643. (g) M. Araki, H. Yamabe, N. Koshikawa, K. Tsukiyama, A. Nakane, T. Okabayashi, A. Kunimatsu, N. Kuze, *Astrophys. J.* 2012, **744**, 1-4. (h) M. Larsson, W. D. Geppert, G. Nyman, *Rep. Prog. Phys.* 2012, **75**, 066901. (i) A. G. G. M. Tielens, *Rev. Mod. Phys.* 2013, **85**, 1021-1081.
7 (a) C. E. Baukal, *Oxygen-enhanced combustion*; CRC Press: New York, 1998. (b) M. J. Piling, D. A. Greenhalgh, A. N. Hayhurst, R. P. Lindstedt, D. B. Smith, I. W. M. Smith, and J. Wolfrum, *Combustion Chemistry: Elementary Reactions to Macroscopic Processes*. London, 2001. (c) The Faraday Division, Royal Society of Chemistry, London, 2002, **119**, 1-475. (d) M. Ray, B. Saha, and G. C. Schatz, *J. Phys. Chem. C* 2012, **116**, 26577-26585.
8 (a) W. Weltner Jr. and R. J. van Zee, *Chem. Rev.* 1989, **89**, 1713-1747. (b) D. C. Parent and S. L. Anderson, *Chem. Rev.* 1992, **92**, 1541-1565. (c) A. V. Order and R. J. Saykally, *Chem. Rev.* 1998, **98**, 2313-2357. (d) C. Lifshitz, *Int. J. Mass Spectrom.* 2000, **200**, 423-442.
9 (a) S. W. McElvany, W. R. Creasy, and A. O'Keefe, *J. Chem. Phys.* 1986, **85**, 632-633. (b) A. O'Keefe, B. I. Dunlap, and S. W. McElvany, *J. Chem. Phys.* 1986, **86**, 715-725. (c) S. W. McElvany, *J. Chem. Phys.* 1988, **89**, 2063-2075. (d) D. Parent and S. W. McElvany, *J. Am. Chem. Soc.* 1989, **111**, 2393-2401.
10 D. C. Parent, *J. Am. Chem. Soc.* 1990, **112**, 5966-5973.
11 J. Sun, H. F. Grutzmacher, and C. Lifshitz, *J. Am. Chem. Soc.* 1993, **115**, 8382-8388.
12 (a) A. B. Raksit and D. K. Bohme, *Int. J. Mass Spectrom. Ion Proc.* 1983, **55**, 6982. (b) D. K. Bohme, A. B. Raksit, and A. Fox. *J. Am. Chem. Soc.* 1983, **105**, 5481. (c) D. K. Bohme, S.

Wlodek, W. Leonard, and A. Fox *J. Chem. Phys.* 1987, **87**, 6934. (d) D. K. Bohme, S. Dheanhanoo, S. Wlodek, and A. B. Raksit, *J. Chem. Phys.* 1987, **91**, 2569. (e) D. K. Bohme and S. Wlodek. *Int. J. Mass Spectrom. Ion Proc.* 1990, **102**, 133.

13 K. Giles, N. G. Adams, D. Smith, *Int. J. Mass Spectrom. Ion Proc.* 1989, **89**, 303.

14 (a) P. A. Hintz, M. B. Sowa, and S. L. Anderson, *Chem. Phys. Lett.* 1991, **177**, 146. (b) M. B. Sowa and S. L. Anderson, *J. Chem. Phys.* 1992, **97**, 8164. (c) M. B. Sowa, J. N. Smolanoff, I. B. Goldman, and S. L. Anderson *J. Chem. Phys.* 1994, **100**, 8784.

15 S. Yang, K. J. Taylor, M. J. Craycraft, J. Conceicao, C. L. Pettiette, O. Cheshnovsky, and R. E. Smalley, *Chem. Phys. Lett.* 1988, **144**, 431.

16 L. Belau, S. E. Wheeler, B. W. Ticknor, M. Ahmed, S. R. Leione, W. D. Allen, H. F. Schaefer III, and M. A. Duncan, *J. Am. Chem. Soc.* 2007, **129**, 10229.

17 (a) P. Freivogel, J. Fulara, D. Lessen, D. Forney, and J. P. Maier, *Chem. Phys.* 1994, **189**, 335. (b) J. P. Maier, *J. Phys. Chem. A* 1998, **102**, 3462. (c) J. Fulara, E. Riaplov, A. Batalov, I. Shnitko, and J. P. Maier, *J. Chem. Phys.* 2004, **120**, 7520. (d) J. Fulara, I. Shnitko, A. Batalov, and J. P. Maier, *J. Chem. Phys.* 2005, **123**, 044305.

18 (a) G. von Helden, M. T. Hsu, P. R. Kemper, and M. T. Bowers, *J. Chem. Phys.* 1991, **95**, 3835. (b) G. von Helden, P. R. Kemper, N. G. Gotts, and M. T. Bowers, *Science* 1993, **259**, 1300. (c) G. von Helden, M. T. Hsu, N. G. Gotts and M. T. Bowers, *J. Phys. Chem.* 1993, **97**, 8182. (d) G. von Helden, N. G. Gotts, and M. T. Bowers, *Chem. Phys. Lett.* 1993, **212**, 241. (f) G. von Helden, N. G. Gotts, and M. T. Bowers, *J. Am. Chem. Soc.* 1993, **115**, 4363. (g) G. von Helden, N. G. Gotts, W. E. Palke, and M. T. Bowers, *Int. J. Mass Spectrom. Ion Proc.* 1994, **138**, 133. (h) N. G. Gotts, G. von Helden and M. T. Bowers, *Int. J. Mass Spectrom. Ion Proc.* 1995, **149/150**, 217. (i) S. Lee, N. G. Gotts, G. von Helden, M. T. Bowers, *J. Phys. Chem. A* 1997, **101**, 2096.

19 K. Koyasu, T. Ohtaki, N. Hori, and F. Misaizu, *Chem. Phys. Lett.* 2012, **523**, 54.

20 R. S. Mulliken, *Phys. Rev.* 1939, **56**, 778-781.

21 K. S. Pitzer and E. Clementi, *J. Am. Chem. Soc.* 1959, **81**, 4477-4485.

22 (a) K. Raghavachari, R. A. Whiteside and J. A. Pople, *J. Chem. Phys.* 1986, **85**, 6623-6628. (b) K. Raghavachari and J. S. Binkley, *J. Chem. Phys.* 1987, **87**, 2191-2197. (c) K. Raghavachari, *Z Phys. D* 1989, **12**, 61-64.

23 S. Shaik, D. Danovich, W. Wu, P. Su, H. S. Rzepa, and P. C. Hiberty, *Nature Chem.* 2012, **4**, 195-200.

24 (a) C. Liang and H. F. Schaefer III, *Chem. Phys. Lett.* 1990, **169**, 150-160. (b) C. Liang, and H. F. Schaefer III, *J. Chem. Phys.* 1990, **93**, 8844-8849. (c) D. H. Magers, R. J. Harrison, and R. J. Bartlett, *J. Chem. Phys.* 1986, **84**, 3284-3290. (d) J. D. Watts, and R. J. Bartlett, *Chem. Phys. Lett.* 1992, **190**, 19-24. (e) D. A. Plattner, and K. N. Houk, *J. Am. Chem. Soc.* 1995, **117**, 4405-4406. (f) J. M. L. Martin, and P. R. Taylor, *J. Phys. Chem.* 1996, **100**, 6047-6056. (g) M. Muhlhauser, G. E. Froudakis, S. D. Peyerimhoff, *Chem. Phys. Lett.* 2001, **336**, 171-176.

25 (a) R. S. Grev, I. L. Alberts, and H. F. Schaefer III, *J. Phys. Chem.* 1990, **94**, 3379-8744. (b) G. v. Helden, N. G. Gotts, W. E. Palke, and M. T. Bowers, *Chem. Phys. Lett.* 1993, **212**, 247-252.

26 M. G. Guiffreda, M. S. Deleuze, J. F. Francois, *J. Phys. Chem. A* 1999, **103**, 5137-5151.

27 G. Orlova, and J. D. Goddard, *Chem. Phys. Lett.* 2002, **363**, 486-491.

28 (a) M. Schnell, M. Muhlhauser, G. E. Froudakis, and S. D. Pyerimhoff, *Chem. Phys. Lett.* 2001, **340**, 559-564. (b) J. Haubrich, M. Muhulhauser, and S. D. Pyerimhoff, *Phys. Chem. Chem. Phys.* 2002, **4**, 2891-2896. (c) J. Haubrich, M. Muhulhauser, and S. D. Pyerimhoff, *J. Mol. Spectros.* 2004, **228**, 31-37. (d) C. Gillery, P. Rosmus, H. J. Werner, H. Stoll, and J. P. Mayer, *Mol Phys.* 2004, **102**, 2227-2236. (e) H. Masso, M. L. Sonent, P. Rosmu, and M. Hochlaf, *J. Chem. Phys.* 2006, **124**, 234304. (f) M. Hochlaf, C. Nicolas, L. Poisson, *J. Chem. Phys.* 2007, **127**, 014310. (g) J. Zhang, X. Guo, and Z. Cao, *J. Chem. Phys.* 2009, **131**, 144307. (h) J. Zhang, X. Guo, and Z. Cao, *Int. J. Mass Spectrom*. 2010, **290**, 113-119. (g) Y. Zhang, L. Wang, Y. Li, and J. Zhang. *J. Chem. Phys.* 2013, **138**, 204303.

29 K. Koyasu, K. Komatsu, and F. Misaizu, *J. Chem. Phys.* 2013, **139**, 164308.

30 (a) J. D. Watts, J. Gauss, and R. J. Bartlett, *J. Chem. Phys.* 1993, **98**, 8718. (b) J. Gauss, W. J. Lauderdale, J. F. Stanton, J. D. Watts, and R. J. Bartlett, *Chem. Phys. Lett*. 1991, **182**, 207. (c) W. J. Lauderdale, J. F. Stanton, J. Gauss, J. D. Watts, and R. J. Bartlett, *Chem. Phys. Lett.* 1991, **187**, 21.

31 J. A. Pople, M. Head-Gordon, and K. Raghavachari, *J. Chem. Phys.* 1987, **87**, 5968.

32 T. H. Dunning, *J. Chem. Phys.* 1989, **90**, 1007.

33 (a) A. D. Becke, *J. Chem. Phys.* 1993, **98**, 5648. (b) C. Lee, W. Yang, and R. G. Parr, *Phys. Rev. B* 1988, **37**, 785.

34 H.-J. Werner, MOLPRO, version 2010.1, a package of ab initio programs, see http://www.mopro.net.

35 (a) T. J. Lee, and P. R. Taylor, *Int J. Quant. Chem.* 1989, **S23**, 199. (b) T. J. Lee, J. E. Rice, G. E. Scuseria, and H. F. Schaefer III, *Theor. Chim. Acta* 1989, **75**, 81. (c) D. Jayatilaka, and T. J. Lee, *J. Chem. Phys.* 1993, **98**. 9734.

36 (a) W. D. Allen, D. A. Horner, R. L. Dekock, R. B. Remingto, and H. F. Schaefer III, *Chem. Phys.* 1989, **113**, 11. (b) E. R. Davidson, and W. T. Borden, *J. Phys. Chem.* 1983, **87**, 4783. (c) T. D. Crawford, J. F. Stanton, W. D. Allen, and H. F. Schaefer, III, *J. Chem. Phys.* 1997, **107**, 10626. (d) M. L. Leininger, C. D. Sherril, W. D. Allen, and H. F. Schaefer, III, *J. Chem. Phys.* 1998, **108**, 6717. (e) C. D. Sherril, M. S. Lee, M. Head-Gordon, *Chem. Phys. Lett.* 1999, **302**, 425. (f) W. Eisfeld, and K. Morokuma, *J. Chem. Phys.* 2000, **113**, 5587. (g) L. Engelbrecht, and B. Liu, *J. Chem. Phys.* 1983, **78**, 3097. (h) A. D. McLean, B. H. Lengsfield III, J. Pacansky, and Y. Ellinger, *J. Chem. Phys.* 1985, **83**, 3567. (i) S. Sen, P. Seal, and S. Charkrabarti, *Phys Rev. B* 2006, **73**, 245401. (j) T. Torelli, and L. Mitas, *Phys. Rev. Lett.* 2000, **85**, 1702. (k) N. J. Russ, T. D. Crawford, and G. S. Tschumper, *J. Chem. Phys.* 2004, **120**, 7298.

37 C. W. Bauschlicher, H. F. Schaefer III, and C. F. Bender, *J. Am. Chem. Soc.* 1976, **98**, 1653.

38 C. W. Bauschlicher, K. Haber, H. F. Schaefer III, and C. F. Bender, *J. Am. Chem. Soc.* 1977, **99**, 3610.

39 R. D. Bach, M. D. Su, E. Aldabbagh, J. L. Andres, and H. B. Schlegel, *J. Am. Chem. Soc.* 1993, **115**, 10237.

40 B. J. Lynch, and D. G. Truhlar, *J. Phys. Chem. A* 2001, **105**, 2936.

41 A. M. Mebel, K. Morokuma, and M. C. Lin *J. Chem. Phys.* 1995, **103**, 3440.